Desalination 396 (2016) 1–16

Contents lists available at ScienceDirect

Desalination

journal homepage: www.elsevier.com/locate/desal

Performance control on adsorption desalination using initial time lag (ITL) of individual beds

Albert S. Kim [a], Ho-Saeng Lee [b], Deok-Soo Moon [b], Hyeon-Ju Kim [b,*]

[a] Civil and Environmental Engineering, University of Hawaii at Manoa, 2540 Dole Street Holmes 383, Honolulu, HI 96822, USA
[b] Seawater Utilization Plant Research Center (SUPRC), Korea Research Institute of Ships & Ocean Engineering, 124-32, Simcheungsu-gil, Jukwang-myeon, Goseong-gun, Gangwon-do 219-822, Republic of Korea

HIGHLIGHTS

- Initial time lag scheme was developed as a novel control factor of adsorption desalination.
- AD performance is investigated in the dual and desalination modes.
- An analytic equation to calculate switching interval is derived.
- Mass balance equation for reaction beds are mathematically generalized.

GRAPHICAL ABSTRACT

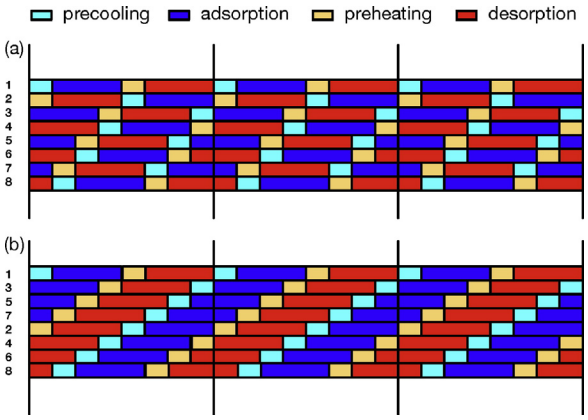

ARTICLE INFO

Article history:
Received 2 March 2016
Received in revised form 3 May 2016
Accepted 4 May 2016
Available online xxxx

Keywords:
Adsorption desalination
Switching interval
Initial time lag (ITL)
Multiple-bed effect
Optimal AD sequence

ABSTRACT

This paper introduces a novel time-scheduling scheme for adsorption desalination (AD). Mathematically, a critical bed pressure of the Toth isotherm is defined as the pressure above which the uptake ratio scarcely changes. Heat balance equations of sorption beds for precooling, adsorption, preheating, and desorption are unified into a single equation. This general governing equation is used to model AD systems, which consists of an arbitrary number of bed pairs with specifically preset initial thermal phases. A theoretical minimum of switching interval is derived as a function of thermal properties of reaction beds and heat exchangers. In the new time scheduling scheme, no bed pairs are in an identical process schedule, because each bed has its initial time lag (ITL) when the operation starts. We found that specific AD performances vary noticeably depending on the ITL values, the number of beds, and more importantly, the number of beds in a time-lag group. There must be an optimal ITL for given operational parameters, which can distinctly increase the water production rate without using extra heat sources. This can dynamically optimize the relative performance of desalination rates and cooling capacities of AD processes.

1. Introduction

Supplies of water, energy and food are vital resources for human living, which are being depleted worldwide. The world's population is

* Corresponding author.
E-mail address: hyeonju@kriso.re.kr (H.-J. Kim).

http://dx.doi.org/10.1016/j.desal.2016.05.004
0011-9164/

now 7.35 billion (B) and is projected to be 8.5 B by 2030 [1]. Current global water requirement is 4500 km^3 (cubic kilometers) annually and will increase to 6900 km^3 by 2030. Water demand is closely related to food production. For example, 1 cal of food requires on the average 1 l of water for production [2], and agriculture accounts for two thirds of global water withdrawal [3]. To meet the ever-increasing global water demand, desalination by thermal and membrane processes can be primary methods [1]. Ideal thermodynamic limit for seawater desalination is 0.78 kWh/m^3, independent of specific thermodynamic processes. Comparative analyses of specific energy consumption of the thermal and membrane processes can be found elsewhere [4–6]. In addition to water demand, global cooling demand also seems to significantly increase with population growth and individual income growth. Cooling degree days (CDD) is often used to estimate the daily cooling demand, defined as the day's average of the highest and lowest temperatures, subtracted by the base temperature (typically set as 65 °F). Annual CDD is calculated as CDD times 365 days. Sivak suggested annual person cooling degree days (APCDD), which is a product of ACDD and a nation's population [7]. The current ACDD and APCDD of the United States are 882 and 278,712, respectively. The total demand in 169 countries (excluding the United States) is currently 45 times greater than that in the United States [8].

The current global situation for water and cooling demands requires an innovative technology that can produce potable water and cooling power flexibly, using renewable and/or inexpensive heat sources. As energy-saving solutions for renewable desalination, AD and membrane distillation recently received close attention [9,10]. Adsorption desalination (AD) can be used for the dual production of potable water and cooling power, and thus be beneficial for regions with hot climates. AD systems are compact, (almost) free from moving parts, and efficiently driven by renewable/inexpensive heat sources. AD consists of non-toxic and environmentally benign materials, requires no synthetic lubricants because it uses only water as the working fluid, and has a low initial cost. AD uses an adsorbent (silica gel) for dynamically alternating adsorption and desorption of an adsorbate (water) using only one heat source. Pairs of beds undergo alternative sub-operations of adsorption/desorption and precooling/preheating. For instance, if bed 1 is in the adsorption (or precooling) phase, paired bed 2 is in the desorption (or preheating) phase. This is because cold and hot water streams for heat exchange are alternatively directed toward the paired beds using a toggle valve. AD does not have a steady state, but phases are systematically coupled and periodically exchanged. The time used for precooling and preheating is the switching interval, and time spent for adsorption and desorption is the reaction time. The sum of these two time scales is a half cycle. Thus, a full cycle consists of two switching intervals and two reaction times.

Ng et al. has compared various refrigeration and desalination systems and reported that a silica-gel/water AD system is one of the most cost-effective and environmentally friendly solutions for desalination and refrigeration [6,11]. Extensive experimental and simulation studies have been performed to investigate the performance of a single stage silica-gel/water AD system for various temperature ranges [12–16]. Previously, Saha et al. showed that the cycle time is an influential parameter on both cooling capacity and coefficient of performance (COP) [17], reporting that the cooling capacity is maximized at a certain cycle time, while the performance increases monotonously with the cycle time. In the same light, Alam et al. reported that the maximum cooling capacity can be achieved by controlling the switching interval [18]. Recently, the potential of AD hybridization the conventional multi-effect distillation (MED) was modeled using thermal energy from the brine heater and extracted vapor stream from the last stage of the MED process at sub-atmospheric pressures and temperatures [19]. A follow-up experimental study supported the model prediction, as attributed to the synergistic operation of the conventional MED and AD systems [20]. On the other hand, an advanced AD cycle was proposed by utilizing an encapsulated evaporator–condenser unit for effective heat transfer and internal heat recovery [15]. Wu et al. theoretically proposed several thermodynamic cycles of AD in terms of temperatures of evaporator and cooling water streams [21] and experimentally validated the new cycles [22]. Their study concluded that the maximum water production rate as well as the minimum energy consumption were achieved by maintaining the evaporator temperature higher than the cooling temperatures of adsorbent and condenser. Thu. et al. applied the concept of multi-effect to AD, and investigated multi-effect adsorption desalination (MEAD) using a single heat source [23]. The performance ratio of the MEAD cycle was reported as high as 6.3 and the cycle-averaged specific water production rate was about 1.0 m3/h per ton of silica gel. Kim et al. investigated the potential of ferroaluminophosphate as a novel adsorbent in a temperature range from 20 °C to 80 °C [24]. A hybrid isotherm consisting of Henr's and Sips' isotherms successfully captured the unique trend of the uptake ratio, i.e., a monotonous increase followed by a sudden jump with respect to the vapor partial pressure. Solar-assisted AD cycle was investigated to assess product water quality [25], reporting that the TDS levels from approximately 40,000 ppm in feed seawater was significantly reduced to <10 ppm.

The above research aimed to improve AD performance by developing multi-stage AD systems of serially connected reaction beds, hybridizing AD with conventional thermal desalination schemes, and utilizing internal heat resources for efficient/additional energy recovery. However, relatively less work has been carried out on understanding effects of initial time lag (ITL) of bed phases, chilling water temperature, and the various number of beds (having the same evaporator and condenser). When multiple pairs of reaction beds are used, the initiation time of each bed pair can be, in principle, independent. For example, when two bed-pairs (of total 4 beds) are initialized, the second pair can start after a certain time after the first bed-pair started pre-processing. This is because operation of each pair is not directly influenced through the common evaporator and condenser. Although scales of reaction and switching times significantly alter the overall performance of various AD systems,in most cases these time scales are empirically determined by trial and error. To the best of our knowledge, no theoretical framework was fully established for determining the switching interval and reaction times. One of the noticeable advantages of an AD system is the simultaneous production of cooling capacity and fresh (distilled) water. As demand for water and cooling can temporarily vary, it is desirable to control the relative production of cooling capacity and fresh water by adjusting the feed temperature of the evaporator and condenser. In this work, we investigate the effects of the number of beds, initial time lag, and input-stream temperatures on the AD performance for optimized simultaneous cooling and desalination.

2. Theory

2.1. Isotherm and bed pressure

2.1.1. Toth isotherm

Toth developed an isosteric isotherm between water as the adsorbate and silica gel as the adsorbent [26]:

$$\phi^* = \frac{K_0 \exp\left[\frac{H_{st}}{RT}\right] P}{\left\{1 + \left[K_0 \exp\left[\frac{H_{st}}{RT}\right] P/\phi_m\right]^{\tau_1}\right\}^{1/\tau_1}} \tag{1}$$

where ϕ^* is the adsorbed quantity of adsorbate, i.e., mass-adsorbate per mass-adsorbent, by the adsorbent under isothermal equilibrium conditions, ϕ_m denotes the monolayer capacity, P is the partial pressure of the adsorbate in gaseous phase, T is the absolute temperature, H_{st} is the

isosteric enthalpy of adsorption, K_0 is the pre-exponential constant, τ_1 is the dimensionless Toth constant, and $\mathcal{R}$ (=8.314 kJ/K mol) is the universal gas constant. Because H_{st} has units of kJ/kg, we used $\mathcal{R}$ = 0.4606350 kJ/kg · K specifically for water with a molecular weight of 18.05 g/mol. For RD silica gel, the parameter values are reported as ϕ_m = 0.45 kg/kg, H_{st} = 2.693 × 10^3 kJ/kg, K_0 = 7.30×10^{-10} kg · kg^{-1} · kPa^{-1}, and τ_1 = 12 [27]. Fig. 1 shows good agreements between theoretical prediction of Eq. (1) and some experimental data reviewed by Ref. [27].

2.1.2. Critical pressure

In Toth's isotherm adsorption uptake, ϕ^* linearly increases for low P and converges to a plateau for high P (see Fig. 1). A transition point between these two regions indicates a specific pressure above which ϕ^* hardly increases. In this work, we named it the critical pressure and calculated it as follows. First, Eq. (1) is re-written as.

$$\phi^* = \frac{\phi_m}{\left\{1+[P/P_0]^{-\tau_1}\right\}^{1/\tau_1}} \tag{2}$$

where

$$P_0 = \frac{\phi_m}{K_0}\exp\left[-\frac{H_{st}}{\mathcal{R}T}\right] \tag{3}$$

which is a sole function of temperature. The critical pressure P_{crit} is obtained by calculating

$$\frac{d^3\phi^*}{dP^3} = 0 \tag{4}$$

because $-d^2\phi^*/dP^2$ must have the shape of a narrow normal distribution. Eq. (4) results in.

$$P_{crit} = 0.980\,P_0 \approx P_0 \tag{5}$$

where specific values of P_0 and P_{crit} are in Table 1. In a practical sense, one can use the critical pressure as the upper-limit of bed pressure during the cyclic operation. In this respect, an advanced AD scheduling can use $P_{crit}(T)$ to dynamically optimize AD performance. This is often practically optimized using proper switching intervals and reaction times.

Table 1
Variation of the critical pressure P_{crit} with respect to temperature.

T[K]	T[°C]	P_0[kPa]	P_{crit}[kPa]
304.15	31.00	2.7670	2.7117
310.15	37.00	4.0134	3.9331
316.15	43.00	5.7395	5.6247
323.15	50.00	8.5672	8.3958
338.15	65.00	19.1148	18.7325

2.1.3. Isosteric pressure

The bed is thermally isolated during the isosteric pre-processing period. The bed pressure is determined by the previous uptake rate ϕ and the current bed temperature T. Therefore, the isosteric bed pressure is represented as an inverse Toth isotherm of Eq. (1):

$$P^* = \frac{\phi\exp\left[-\frac{H_{st}}{RT}\right]}{K_0\left\{1-[\phi/\phi_m]^{\tau_1}\right\}^{1/\tau_1}} \tag{6}$$

2.1.4. Adsorption dynamics

The uptake rate of water by the silica gel is obtained using a driving force equation as.

$$\frac{d\phi}{dt} = k_s a_v(\phi^*-\phi) \tag{7}$$

$$k_s a_v = \frac{15D_s}{R_p^2} \tag{8}$$

$$D_s = D_{s0}\exp\left(-\frac{E_a}{RT}\right) \tag{9}$$

where $k_s a_v$ is the effective mass transfer coefficient, R_p is the silica gel radius, D_s is the surface diffusion coefficient, D_{s0} is the kinetic constant having the diffusivity unit, and E_a is the activation energy. Specific parameter values for the uptake rate are taken from Ref. [28] and listed in Table 2.

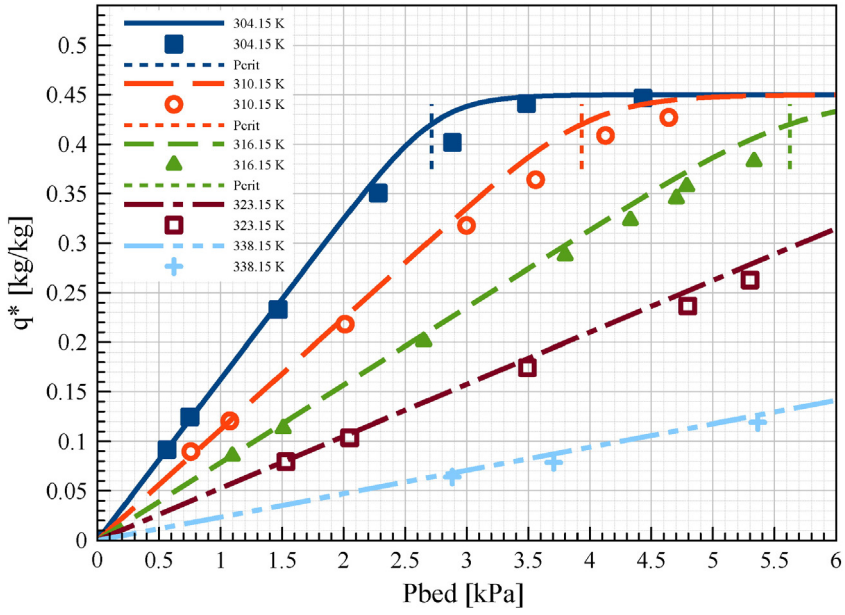

Fig. 1. The equilibrium adsorption uptake, ϕ^*, as a function of refrigerant temperature and pressure at gaseous equilibrium. Lines and symbols indicate theoretical and experimental results, respectively.

Table 2
Parameter values used for adsorption desalination simulations [28]. For dual-use and desalination modes, $T_{ch,in}$ = 15 °C and 30 °C are employed, respectively.

Evaporator			Condenser		
$M_{ff,evap}$	12.00	kg	$M_{ff,cond}$	24.00	kg
$M_{hx,evap}$	6.00	kg	$M_{hx,cond}$	4.00	kg
$c_{p,hx,evap}$	0.48	kJ/kg K	$c_{p,hx,cond}$	0.48	kJ/kg K
U_{evap}	2.00	kW/m^{2}K	U_{cond}	0.08	kW/m2K
A_{evap}	0.08	m^2	A_{cond}	0.60	m2
$\dot{m}_{ch}$	0.21	kg/s	$\dot{m}_{cf}$	0.60	kg/s
$T_{ch,in}$	15.00	°C	$T_{cf,in}$	30.00	°C
Beds			**Silica gel**		
M_{sg}	5.60	kg	D_{s0}	2.54×10^{-4}	m2/s
$M_{hx,bed}$	11.00	kg	E_a	42.00	kJ/mol
$c_{p,hx,bed}$	0.48	kJ/kg K	$c_{p,sg}$	0.921	kJ/kg K
U_{bed}	0.25	kW/m^{2}K	R_p	80.0	μm
A_{bed}	0.54	m^2	H_{st}	2693.00	kJ/kg
$\dot{m}_{cw}$	0.21	kg/s	ϕ_m	0.45	kg/kg
$\dot{m}_{hw}$	0.21	kg/s	τ	12	[−]
$T_{hw,in}$	85.0	°C	K_0	7.30×10^{-10}	kg/kg kPa
$T_{cw,in}$	30.0	°C			

2.2. Timing schedule

Fig. 2 shows the timing schedule for a pair of beds in opposite phases. The switching interval for precooling and preheating is assumed to be equal, while the duration for adsorption and desorption is given by the pre-set reaction time. Initially, beds 1 and 2 are in the first switching period for the precooling and preheating phases, respectively, and connected to neither the evaporator nor the condenser. In the first reaction period, bed 1 adsorbs the vapor flow from the evaporator, and bed 2 desorbs the pre-adsorbed water to the condenser. The first half cycle consists of the switching interval plus the reaction time of Fig. 2(a) and (b), respectively. In the second half cycle, roles of beds 1 and 2 are exchanged as shown in Fig. 2c and (d), respectively. During the full cycle, a bed exchanges heat from the cold input stream for precooling and adsorption, and utilizes heat from the hot input stream for preheating and desorption. This connection/isolation scheme is symmetric on the bed index. In other words, exchanging the bed index ($1 \leftrightarrow 2$) does not affect the thermal loads of the evaporator and condenser. When more than two paris of beds are used for AD, at most a half of the total beds are simultaneously connected to the evaporator (or the condenser).

2.3. Thermodynamic mechanism

The relationship between pressure and temperature is described by the Clausius-Clapeyron equation for equilibrium of two thermodynamic states of different phases:

$$\ln P = -\frac{\Delta h}{R_g}\frac{1}{T} + \text{constant} \tag{10}$$

where Δh is the enthalpy for the phase change. In Eq. (10), ln P can be plotted with respect to $-T^{-1}$, as shown in Fig. 3. The full cycle of adsorption desalination consists of two isosteres and two isobars that intersect at points determined by temperatures of T_A to T_F. The Clausius-Clapeyron equation above may be represented for water as

$$\ln\frac{P}{P_0} = -\frac{L(T)}{R_g T}$$

where $P_0 = 3.622236 \times 10^{23}$ kPa and $L(T) = l_0 - l_1 T$ is the latent heat of water where $l_0 = 3168.14$ kJ/kg and $l_1 = 2.43448$ kJ/kg · K [29].

Bed 1 of Fig. 2 undergoes the following cycle in sequence as its thermodynamic state is shown in Fig. 3:

1. After the bed finishes the desorption process, it is isolated from both the evaporator and the condenser. Precooling follows to decrease the bed temperature for adsorption. In this isosteric precooling process [$D \rightarrow F$], the bed temperature decreases from T_D to T_F while the uptake ratio in the bed is kept constant as ϕ_D (see the state of bed 1 in Fig. 2(a)). As the bed temperature decreases, entropy decreases:

$$dS_{pcl}\ (<0) = \left(\frac{c_{p,s} + c_{p,a}}{T}\right)dT - \left(\frac{\partial v_a}{\partial T}\right)_{P,\phi} dP \tag{11}$$

   where pressure decreases from P_{cond} to P_{evap}. See Appendix A for details.
2. During the adsorption process [$F \rightarrow A$], the adsorbate (water) is evaporated at (often low) pressure P_{evap} and temperature T_{evap} in the evaporator and transported to the adsorption bed due to the enthalpy gradient. The adsorbate is then adsorbed into the pores of the adsorbent (silica gel) under the isobaric conditions at $P_{bed} = P_{evap}$. The adsorption heat is released during phase change and removed by a heat exchanger (installed inside the bed) having the cooling water stream of temperature T_{cw}. The bed temperature gradually decreases from T_F to T_A and the uptake increases from $\phi_F \approx \phi^*(P_{evap}, T_F)$ to

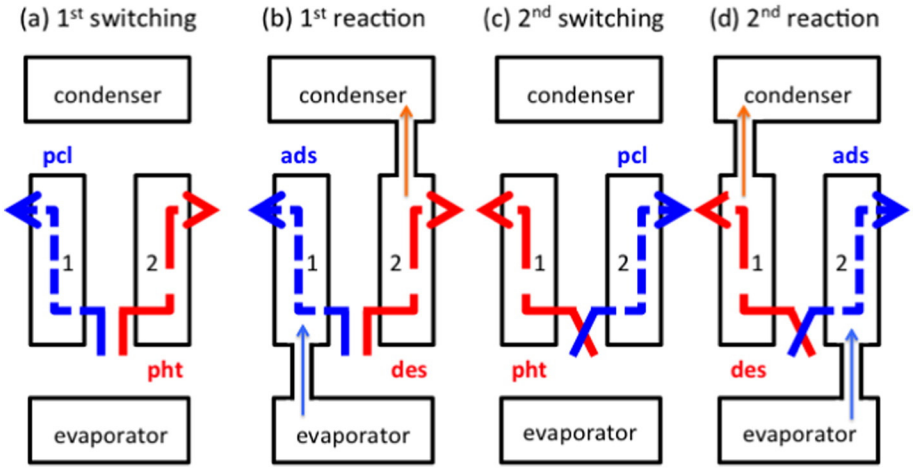

Fig. 2. Timing of four subprocesses of two-bed adsorption desalination.

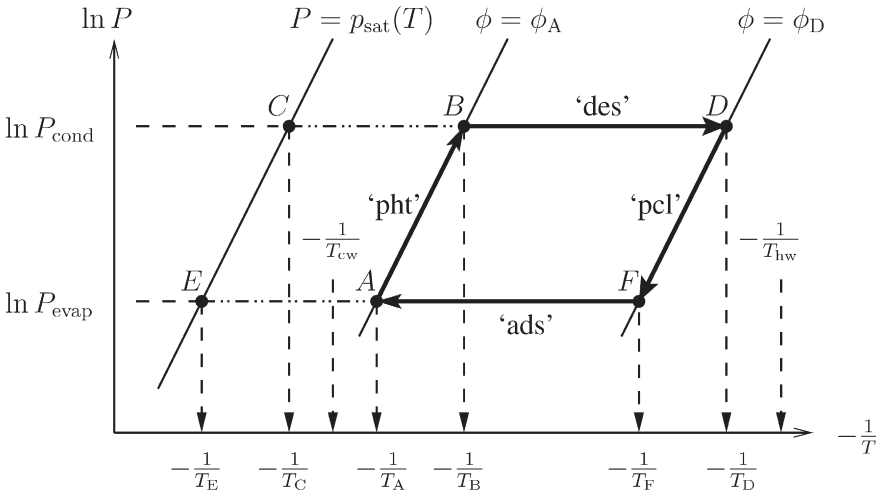

Fig. 3. P–T–ϕ diagram.

$\phi_A \approx \phi^*(P_{evap},T_A)$. The adsorption uptake rate can be represented in differential form as

$$\frac{d\phi_{ads}(t)}{dt} = k_s a_v(T_{bed})\ [\phi^*(P_{evap},T_{bed}) - \phi_{ads}(t)] \tag{12}$$

As the bed temperature decreases, the maximum uptake $\phi^*(P_{evap},T_{bed})$ increases, maintaining a positive uptake rate, $\dot{\phi}_{ads}$. (See the state of bed 1 in Fig. 2(b).) During adsorption, the bed temperature gradually decreases because of the phase change of the adsorbate from a gas to adsorbed phases. Therefore, adsorption entropy decreases with temperature while ϕ increases:

$$dS_{ads}\ (<0) = \left(\frac{c_{p,s}+c_{p,a}}{T}\right)dT + \left[S_g - \frac{H_{st}}{T}\right]d\phi \tag{13}$$

During precooling and adsorption periods, entropy decreases since the cooling stream decreases the bed temperature.

3. After the silica gel is saturated at point A, the chamber is convectively isolated and becomes subject to isosteric heating for desorption. During this preheating process [$A \rightarrow B$] (see the state of bed 1 in Fig. 2(c)), the bed pressure increases from P_{evap} to P_{cond}, and ϕ is maintained at its isosteric value at the end of the adsorption, $\phi_A = \phi^*(P_{evap},T_A)$. As the uptake isotherm depends on the equilibrium temperature and pressure in the bed, the pressure can be inversely calculated as a function of temperature using the isotherm in this isosteric phase, making the path line from A to B. Entropy increases in this preheating phase as much as it decreases in the precooling phase

$$dS_{pht} = -dS_{pcl} > 0 \tag{14}$$

as explained in Eq. (11).

4. When the bed pressure reaches the condenser pressure, the bed opens to the condenser to start the isobaric desorption process. During this process [$B \rightarrow D$], the bed pressure is maintained equal to the condenser pressure P_{cond}, and the bed temperature increases from T_B to T_D by utilizing the heat of hot water of temperature T_{hw}, from the heat exchanger. The pre-adsorbed adsorbate is expelled endothermally from the pore surfaces of the silica gel and transferred to the condenser for saturation. The uptake ratio decreases from $\phi_B \approx \phi^*(P_{cond},T_B)$ to $\phi_D \approx \phi^*(P_{cond},T_D)$, and the desorption uptake rate may be represented as

$$\frac{d\phi_{des}(t)}{dt} = k_s a_v(T_{bed})\ [\phi^*(P_{cond},T_{bed}) - \phi_{des}(t)] \tag{15}$$

As the bed temperature increases, the maximum uptake ratio $\phi^*(P_{cond},T_{bed})$ decreases, giving the negative uptake rate, $\dot{\phi}_{des} < 0$. The remaining amount of adsorbate in the silica gel continuously decreases until the end of this desorption process. In the condenser, the adsorbate in the gas phase is being saturated (condensed) at P_{cond}, which is the vapor pressure of water at the condenser temperature T_{cond}. Lowering condenser temperature will enhance the saturation rate and therefore increase the desalination capability, but would require extra energy consumption for cooling. Consequently, use of water or air at the ambient temperature must be a good option to make AD more cost-effective, depending on the relative importance of desalination to cooling (see the state of bed 1 in Fig. 2(d)). Entropy gradually increases in this desorption phase as much as it decreases in the adsorption phase:

$$dS_{des} = -dS_{ads} > 0 \tag{16}$$

as explained in Eq. (13).

5. Before the next adsorption, the silica gel is cooled down isosterically at $\phi^*(P_{cond},T_D)$ until the bed pressure decreases from P_{cond} to P_{evap}. The adsorbate is re-fed from the evaporator. This is identical to step 1 described above. In the full AD cycle describe above, the net entropy change is derived as zero

$$dS_{tot} = 0 \tag{17}$$

as described in detail in Eq. (76). However, this isentropic approximation is based on the assumption that the intrinsically transient AD subprocesses promptly reach local equilibrium states within a time duration much shorter than the half cycle period. In actual AD applicaitons, overall entropy increases in each full cycle, i.e., $dS > 0$. See Appendix A for details.

2.4. Energy balance

In this section, we represent energy balance equations for an arbitrary number of bed pairs, having an even number of total beds. At any time, a bed is assumed to be in local thermodynamic equilibrium.

2.4.1. Evaporator

The energy balance of the evaporator in communication with adsorber beds is

$$(Mc_p)_{\text{evap}}\frac{dT_{\text{evap}}}{dt}=-\sum_{i=1}^{N_{\text{bed}}}M_{\text{sg}}h_{\text{fg}}(T_{\text{evap}})\frac{d\phi_i}{dt}\delta_{S(i),\text{ads}}-\dot{m}_{\text{ch}}c_{\text{p,w}}(T_{\text{ch,out}}-T_{\text{ch,in}}) \tag{18}$$

where $(Mc_p)_{\text{evap}}$ is the effective thermal mass of the evaporator, calculated as a sum of those of feed fluid and heat exchanging substance of the evaporator

$$(Mc_p)_{\text{evap}}=M_{\text{ff,evap}}c_{\text{p,w}}+M_{\text{hx,evap}}c_{\text{p,hx,evap}} \tag{19}$$

and $h_{\text{fg}}(T_{\text{evap}})$ is the evaporation enthalpy of water at T_{evap}. In Eq. (18), the Dirac delta function is specifically defined as

$$\delta_{S(i),\text{ads}}=\begin{cases}1 & \text{if } S(i)=\text{ads}\\ 0 & \text{otherwise}\end{cases} \tag{20}$$

where $S(i)$ indicates the thermodynamic status of bed i, which can be one of 'ads', 'des', 'pcl', and 'pht'. The summation on the right side of Eq. (18) runs over adsorber beds only. The output temperature of the chilled water is represented using the log-mean temperature difference (LMTD) approach, which is

$$T_{\text{ch,out}}=T_{\text{evap}}+(T_{\text{ch,in}}-T_{\text{evap}})\exp\left[-\frac{U_{\text{evap}}A_{\text{evap}}}{\dot{m}_{\text{ch}}c_{\text{p,w}}}\right] \tag{21}$$

The evaporator is assumed to be at any time in equilibrium with the adsorber beds. Identities (indexes) of these beds connected to the evaporator change periodically with respect to the switching interval and reaction time. During reaction periods, the number of adsorber and desorber beds are (usually) equal to the half of the total bed number: $N_{\text{bed,ads}}=N_{\text{bed,des}}=\frac{1}{2}N_{\text{bed}}$. The evaporator temperature at time t can be calculated by integrating Eq. (18):

$$T_{\text{evap}}(t)=T_{\text{evap}}(0)+\int_0^t\dot{T}_{\text{evap}}(t')\ dt' \tag{22}$$

where $T_{\text{evap}}(0)$ is the initial evaporator temperature. The evaporator capacity is often presumed to be large enough to have the pressure of an adsorber bed equal to the saturation pressure at T_{evap}:

$$P_{\text{bed,ads}}=P_{\text{evap}}=p_{\text{sat}}(T_{\text{evap}}) \tag{23}$$

2.4.2. Condenser

The energy balance of the condenser in communication with desorber beds is

$$(Mc_p)_{\text{cond}}\frac{dT_{\text{cond}}}{dt}=-\sum_{i=1}^{N_{\text{bed}}}M_{\text{sg}}h_{\text{fg}}(T_{\text{cond}})\frac{d\phi_i}{dt}\delta_{S(i),\text{des}}-\dot{m}_{\text{ff,cond}}c_{\text{pa}}(T_{\text{air,out}}-T_{\text{air,in}}) \tag{24}$$

where $h_{\text{fg}}(T_{\text{cond}})$ is the evaporation enthalpy of water at T_{cond}, and $(Mc_p)_{\text{cond}}$, similar to Eq. (19), is the effective thermal mass of the condenser, calculated as

$$(Mc_p)_{\text{cond}}=M_{\text{ff,cond}}c_{\text{p,w}}+M_{\text{hx,cond}}c_{\text{p,hx,cond}} \tag{25}$$

In this work, air is selected as a cooling fluid for the condenser, having the specific heat capacity, $c_{\text{p,a}}$. The output temperature of the condenser is similar to Eq. (21),

$$T_{\text{air,out}}=T_{\text{cond}}+(T_{\text{air,in}}-T_{\text{cond}})\exp\left[-\frac{U_{\text{cond}}A_{\text{cond}}}{\dot{m}_{\text{air}}c_{\text{pa}}}\right] \tag{26}$$

and the condenser temperature at time t is calculated by integrating Eq. (24):

$$T_{\text{cond}}(t)=T_{\text{cond}}(0)+\int_0^t\dot{T}_{cond}(t')\ dt' \tag{27}$$

where $T_{\text{cond}}(0)$ is the initial condenser pressure. The pressure of the desorber beds is equal to that of the condenser, which is the saturation pressure at T_{cond}, i.e.,

$$P_{\text{bed,des}}=P_{\text{cond}}=p_{\text{sat}}(T_{\text{cond}}) \tag{28}$$

2.4.3. Reaction bed

2.4.3.1. Precooling and adsorption. The energy balance of a bed under the precooling ($\dot{\phi}=0$) and adsorption ($\dot{\phi}>0$) phases may be represented as:

$$[M_{\text{bed}}c_{\text{p,bed}}+M_{\text{sg}}\phi c_{\text{p,w}}]\frac{dT_{\text{bed}}}{dt}=+\theta_{\text{ads}}M_{\text{sg}}\dot{\phi}[h_{\text{g}}(P_{\text{evap}},T_{\text{bed}})-h_{\text{fg}}(T_{\text{evap}})+H_{\text{st}}]-\dot{m}_{\text{cw}}c_{\text{p,w}}(T_{\text{cw,out}}-T_{\text{cw,in}}) \tag{29}$$

where the effective thermal mass of the bed is

$$(Mc_{\text{p}})_{\text{bed}}=M_{\text{sg}}c_{\text{p,sg}}+M_{\text{hx,bed}}c_{\text{p,hx,bed}} \tag{30}$$

and the output temperature of the cold water for heat exchanging is similar to those of the evaporator and the condenser,

$$T_{\text{cw,out}}=T_{\text{bed}}+(T_{\text{cw,in}}-T_{\text{bed}})\exp\left[-\frac{(UA)_{\text{bed}}}{(\dot{m}c_{\text{pw}})_{\text{cw}}}\right] \tag{31}$$

In the precooling phase, the bed is thermally isolated and the cold stream of the heat exchanger continuously takes heat stored during the previous desorption step. The temperature rapidly decreases in this isosteric process and so does the bed pressure,which follows the inverse isotherm relationship. In the adsorption phase, the heat is released for phase change of the adsorbate so that the bed temperature decreases slowly in comparison to that in the pre-cooling state. The bed pressure remains equal to the evaporator pressure, and the uptake ratio $\dot{\phi}$ increases as ϕ^* increases with the decreasing bed temperature. These two phases can be mathematically represented by Eq. (29) using an on-off function:

$$\theta_{\text{ads}}=\begin{cases}0 & \text{for precooling}\\ 1 & \text{for adsorption}\end{cases} \tag{32}$$

and the specific bed pressure

$$P_{\text{bed}}=\begin{cases}P^*\left(\phi_{\text{pcl}},T_{\text{bed}}\right) & \text{for pre-cooling}\\ P_{\text{evap}} & \text{for adsorption}\end{cases} \tag{33}$$

where P^* is calculated using Eq. (6).

2.4.3.2. Preheating and desorption. The energy balance of the bed under the preheating ($\dot{\phi}=0$) and desorption ($\dot{\phi}<0$) states is represented similarly as

$$[(Mc_{\text{p}})_{\text{bed}}+M_{\text{sg}}c_{\text{pw}}\phi]\frac{dT_{\text{bed}}}{dt}=+\theta_{\text{des}}M_{\text{sg}}\dot{\phi}[h_{\text{g}}(P_{\text{cond}},T_{\text{bed}})-h_{\text{fg}}(T_{\text{cond}})+H_{\text{st}}]-\dot{m}_{\text{hw}}c_{\text{pw}}(T_{\text{hw,out}}-T_{\text{hw,in}}) \tag{34}$$

where the output temperature of the hot water from the heat-exchanging is

$$T_{\text{hw,out}}=T_{\text{bed}}+(T_{\text{hw,in}}-T_{\text{bed}})\exp\left[-\frac{(UA)_{\text{bed}}}{(\dot{m}c_{\text{pw}})_{\text{hw}}}\right] \tag{35}$$

In the preheating phase, the bed is thermally isolated (similar to the precooling phase) and maintained at an isosteric pressure of P^*-(ϕ_{pht},T_{bed}). The uptake ratio, ϕ_{pht}, remains constant after the previous adsorption state. In this desorption state, the latent heat for the phase change is supplied by the incoming hot water from the heat exchanger and the bed is in equilibrium with the condenser of pressure P_{cond}. Similar to Eqs. (32) and (33), we write

$$\theta_{des} = \begin{cases} 0 & \text{for preheating} \\ 1 & \text{for desorption} \end{cases} \tag{36}$$

and

$$P_{bed} = \begin{cases} P^*\left(\phi_{pht}, T_{bed}\right) & \text{for preheating} \\ P_{cond} & \text{for desorption} \end{cases} \tag{37}$$

2.4.3.3. General representation of bed energy balance. The ith bed is at any time in one of the four phases, i.e., pcl, ads, pht, and des, described above. A generalized energy balance equation for Eqs. (29) and (34) is

$$\begin{aligned}\left[(Mc_p)_{bed} + M_{sg}\phi^{(i)}c_{p,w}\right]\frac{dT_{bed}^{(i)}}{dt} = &+\theta_{srp}M_{sg}\dot{\phi}^{(i)}\left[h_g\left(P_{ref}, T_{bed}^{(i)}\right) - h_{fg}(T_{ref}) + H_{st}\right] \\ &-\theta_{cw}\dot{m}_{cw}c_{p,w}\left(T_{cw,out}^{(i)} - T_{cw,in}\right) \\ &-\theta_{hw}\dot{m}_{hw}c_{p,w}\left(T_{hw,out}^{(i)} - T_{hw,in}\right)\end{aligned} \tag{38}$$

where subscript 'ref' will be replaced by 'evap' and 'cond' for adsorption and desorption states, respectively, and specific on/off θ-functions are defined in Table 3.

2.4.4. Output water

At any time, the cold (and hot water) stream goes to $\frac{1}{2}N_{bed}$ beds of precooling/adsorption (and preheating/desorption). The average output temperatures of the cold and hot water from $\frac{1}{2}N_{bed}$ beds are

$$\langle T_{cw,out}\rangle = \frac{2}{N_{bed}}\sum_{i=pcl,ads} T_{cw,out}^{(i)}$$

and

$$\langle T_{hw,out}\rangle = \frac{2}{N_{bed}}\sum_{i=pht,des} T_{hw,out}^{(i)}$$

respectively. Thermal blending of hot (and cold) output streams from reaction beds is assumed to be instantaneous in our theory.

2.5. Performance evaluations

The coefficient of performance (COP) is defined as a ratio of the heat input rate to the evaporator and that to desorption beds:

$$COP = \frac{\langle Q_{evap}\rangle}{\langle Q_{in}\rangle} \tag{39}$$

where

$$Q_{evap} = \dot{m}_{ch}c_{p,w}\left(T_{ch,in} - T_{ch,out}\right) \tag{40}$$

Table 3
Values of on-off functions at the four phases of precooling, adsorption, preheating, and desorption.

	pcl	ads	pht	des
θ_{srp}	0	1	0	1
θ_{cw}	1	1	0	0
θ_{hw}	0	0	1	1

and

$$Q_{in} = \dot{m}_{hw}c_{p,w}\left(T_{hw,in} - T_{hw,out}\right) \tag{41}$$

In Eq. (39), the bracket indicates the time average over the full cycle, i.e.,

$$\langle\cdots\rangle = \frac{1}{T_{cyc}}\int_0^{T_{cyc}}(\cdots)\ dt$$

The specific cooling capacity (SCC) is defined as the cooling capacity $\langle Q_{evap}\rangle$ divided by total mass of silica gel in the beds:

$$SCC = \frac{\langle Q_{evap}\rangle}{M_{sg}N_{bed}} \tag{42}$$

In AD, the amount of water produced per day per unit adsorbent mass is a practically important value, and estimated using the specific daily water production (SDWP) defined as

$$SDWP = \frac{\tau_{day}}{N_{bed}}\left\langle\sum_i \dot{\phi}_{des}^{(i)}\right\rangle \tag{43}$$

where τ_{day} is a day in seconds.

2.6. Specific time scales

2.6.1. Preprocessing time interval

The energy balance Eq. (34) for preheating can be written as

$$\frac{dT_{bed}}{T_{bed} - T_{hw,in}} = -\frac{dt}{\tau_{pht}} \tag{44}$$

where τ_{pht} is interpreted as the characteristic time-scale for preheating, defined as

$$\tau_{pht} = \frac{(Mc_p)_{bed} + M_{sg}c_{pw}\phi_{pht}}{\dot{m}_{hw}c_{pw}(1 - e^{-u_{hw}})} \tag{45}$$

where

$$u_{hw} = -\frac{(UA)_{bed}}{\dot{m}_{hw}c_{cp,hw}} \tag{46}$$

Because the preheating is an isosteric process, ϕ_{pht} in Eq. (45) is equal to that at the end of adsorption state, which is the maximum uptake ratio during all of the steady cycles. Similar to Eq. (45), the characteristic time scale for precooling can be written by simply replacing subscripts 'pht' and 'hw' of Eqs. (45) and (46) with 'pcl' and 'cw', respectively. During the desorption period, ϕ decreases to its minimum, denoted as ϕ_{pcl}, and stays constant during the precooling phase.

If the hot and cold water streams have the same mass flow rate, i.e., $\dot{m}_{cw} = \dot{m}_{hw}$ or equivalently the same thermal mass, i.e., $\dot{m}_{cw}c_{pw} = \dot{m}_{hw}c_{pw}$, then the switching time τ_{sw} can be determined as an average of τ_{pht} and τ_{pcl}, i.e.,

$$\tau_{sw} = \frac{1}{2}\left(\tau_{pht} + \tau_{pcl}\right) = \tau_{sw,bed} + \tau_{sw,water} \tag{47}$$

$$\tau_{sw,bed} = \frac{(Mc_p)_{bed}}{\dot{m}c_{pw}(1 - e^{-u})} \tag{48}$$

$$\tau_{sw,water} = \frac{M_{sg}c_{pw}\overline{\phi}_{sw}}{\dot{m}c_{pw}(1 - e^{-u})} \tag{49}$$

where $u = u_{hw} = u_{cw}$. In above equations, $\tau_{sw,bed}$ is the characteristic time required to change the temperature of the bed consisting of silica gel and

heat-exchanging substance, and $\tau_{sw,water}$ is the characteristic mean time to change the temperature of adsorbed water of average mass $M_{sg}\overline{\phi}_{sw}$, where $\overline{\phi}_{sw} = \frac{1}{2}(\phi_{pht} + \phi_{pcl})$ is the average uptake ratio of preheating and precooling periods. Because silica gel (heat-exchanging substance) and adsorbed water are simultaneously heated up or cooled down, separation of the switching time τ_{sw} into the two components does not give extra meaning. Eqs. (47) and (48) imply, however, that $\tau_{sw,bed}$ is conceptually the theoretical minimum of the switching interval. If a switching time is arbitrarily set less than $\tau_{sw,bed}$, then the heat applied is not enough to change the temperature of the (dry) bed only (excluding adsorbed water in the silica gel). If the half cycle is set to be long enough, then ϕ_{pht} and ϕ_{pcl} will approach to ϕ^*_{max} and zero, respectively, giving $\overline{\phi}_{sw} = \frac{1}{2}\phi^*_{max}$. However, this approximation takes extreme values of ϕ_{pht} and ϕ_{pcl} regardless of specific operation conditions and provides only the theoretical maximum of $\tau_{sw,water}$. To reasonably estimate $\tau_{sw,water}$, one should use optimal values of ϕ_{pht} and ϕ_{pcl} by trial and error.

2.6.2. Time phase shift

Fig. 4 shows the three full cycles of a four-bed AD process. The vertical dotted-lines indicate half-cycle times of the full cycles. Initial states of beds 1 to 4, as shown, are precooling, preheating, adsorption, and desorption, respectively. The phase sequences of beds 1 and 2 during the first full cycle are equal to those of two beds shown in Fig. 2. One can notice that the phase of bed 3 (and 4) at tme t matches exactly to that of bed 1 (and 2) at time $t + \tau_{sw}$, which is mathematically described as

$$S_{i+2}(t) = S_i(t + \tau_{sw}) \tag{50}$$

for $i = 1,2$. In other words, if time t of beds 1 and 2 are shifted by $-\tau_{sw}$ (by replacing t by $t - \tau_{sw}$), then the first group (of beds 1 and 2) and the second group (of beds 3 and 4) will be in the exactly the same thermal phases. It would be interesting to see how the AD performances vary if we set $S_{i+2}(t) = S_i(t + k_{sw}\tau_{sw})$ for an arbitrary positive integer $k_{sw} \le \tau_{hc}/\tau_{sw} - 1$.

We investigate specific cases that the half cycle τ_{sw} is a multiple of switching time τ_{sw}:

$$\tau_{hc} = n_{sw}\tau_{sw} \tag{51}$$

equivalently

$$\tau_{srp} = (n_{sw} - 1)\tau_{sw} \tag{52}$$

where n_{sw} is an integer value. For example, Fig. 5 shows phase sequences of 8 sorption beds with $n_{sw} = 4$, and therefore sorption time and the half cycle are $\tau_{srp} = 3\tau_{sw}$ and $\tau_{half-cyc} = 4\tau_{sw}$ respectively. Potential advantages of using the time interval condition of Eq. (51) are as follows. At any time t, hot water streams are supplied to n_{sw} beds, one for preheating and $n_{sw} - 1$ for desorption, shown in yellow and red bars, respectively, in Fig. 5(a) and (b). Each of the $n_{sw} - 1$ desorption beds supplies hot vapor flow to the condenser, and the condenser at any time receives $n_{sw} - 1$ vapor streams. On the other hand, cooling water streams go to another set of n_{sw} beds, one for precooling and $n_{sw} - 1$ for adsorption. The evaporator provides vapor streams to $n_{sw} - 1$ beds at any time. During the full cycle operation, one set of $n_{sw} - 1$ beds is connected to the evaporator and another set to the condenser. In our opinion, Eq. (51) can be a proper condition to stabilize the thermal loads and performance of the evaporator and condenser.

In Fig. 5(a), there are four bed groups ($N_g = 4$), each consisting of two beds. For example, the first group has beds 1 and 2, the second group has beds 3 and 4, and so forth. Generally speaking, group $i_g (= 1 - 4)$ contains bed $2i_g - 1$ and $2i_g$, of which phases paired are thermally opposite, i.e., precooling and preheating or adsorption and desorption, respectively. In this work, a bed pair consists of two beds of typically consecutive indexes and a bed group can be composed of any even number of beds. Here, we defined the physical pair index of bed i, which is always in an opposite thermal phase to that of bed i. For example, beds 1 & 2, 3 & 4, and so forth are physical pairs of each other, respectively. Therefore, if the bed index i is odd, then its physical pair has an index of $i + 1$; and if i is even, its physical pair has an index of $i - 1$. Therefore, one can define the index of a physical pair of bed i as

$$\mathbb{P}(i) = 2\,\mathrm{mod}(i,2) - 1 = \begin{cases} i+1 & \text{if } i = \text{odd} \\ i-1 & \text{if } i = \text{even} \end{cases} \tag{53}$$

where mod(i,2)indicates a remainder of i divided by 2, which gives 0 and 1 if i is even and odd, respectively. In addition, we supplementarily define the identity operator as

$$\mathbb{I}(i) = i \tag{54}$$

for an arbitrary bed number i. The temporal phase difference between bed groups 1 and 2 is τ_{sw}, and that between bed groups 1 and 3 is $2\tau_{sw}$. One can generalize this relationship between beds i and i'as

$$\Delta\tau_{sw}(i,i') = \tau_{sw} \cdot (i' - i) \tag{55}$$

for $|i - i'| \le n_{sw}$where $i,i' = 1 - 8$. This indicates that the thermal phase of bed i after $\tau_{sw} \cdot (i' - i)$ is equal to the current thermal phase of bed i. Fig. 5(b) shows the same temporal sequences of the 8 beds in Fig. 5(a), reorganized by the thermal phase. Bed 1 is found on the top in both Fig. 5(a) and (b), but beds 2 and 7 in Fig. 5(a) are found in the fifth and fourth ranks in Fig. 5(b), respectively. The ith bed in Fig. 5(a) is ranked jth in Fig. 5(b), where the rank j is calculated as

$$j = 2\left(i - 4\left\lfloor\frac{i}{4}\right\rfloor\right) - 1 + \left\lfloor\frac{i-1}{4}\right\rfloor \tag{56}$$

using a floor operator of x, denoted ⌊x⌋, which gives the greatest integer less than x. It would be useful to identify bed k, which is a temporal phase of bed i after bed i advances $j\tau_{sw}$ in time. This specific bed index is defined as

$$k_{ij} = \begin{cases} \mathbb{I}(k) & \text{if } \kappa \le 8 \\ \mathbb{P}(k) & \text{if } \kappa > 8 \end{cases} \tag{57}$$

where most importantly κ is found as

$$\kappa = \mathrm{mod}(i + 2j - 1, 8) + 1 \tag{58}$$

Table 4 shows values of k_{ij} for $i,j = 1 - 8$. By definition, k_{ij} has the following special characteristic:

$$k_{i0} = k_{i8} = i \tag{59}$$

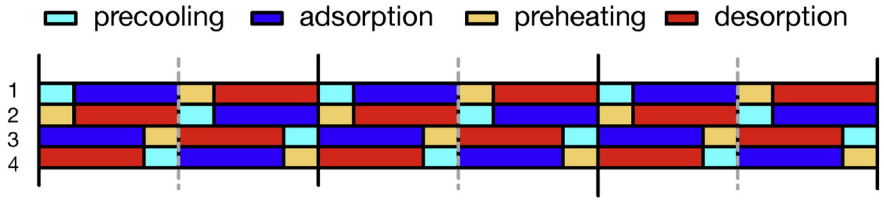

Fig. 4. Phase sequence of four sorption beds in three full cycles.

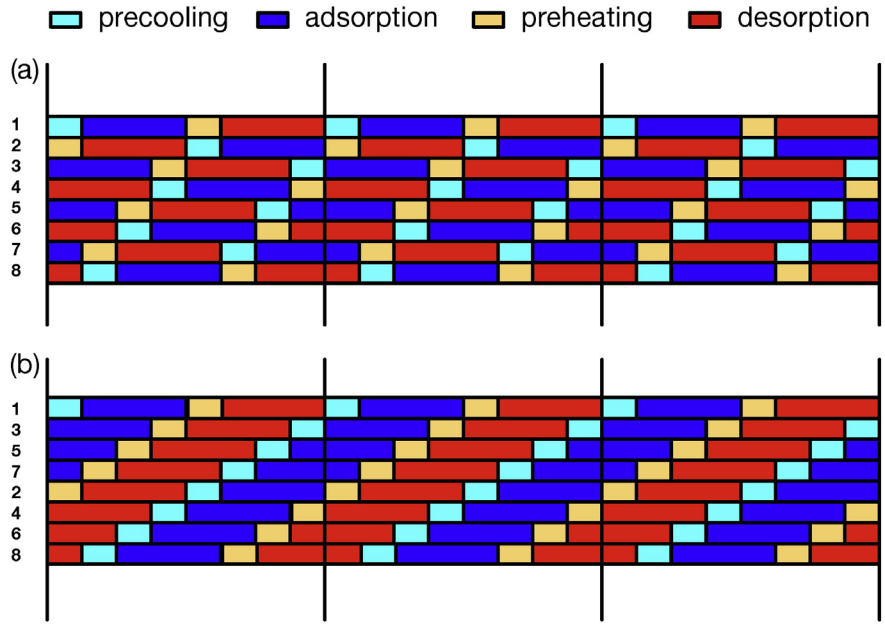

Fig. 5. Phase sequence of sorption for 8 beds in adsorption desalination organized by (a) the intrinsic bed index ($i = 1 - 8$), and (b) temporal sequences of index $1 \le j \le 8$.

because the thermal phase of bed i of no temporal switch should be equal to that of bed i itself after a full cycle. For an arbitrary n_{sw}, Eqs. (56)–(58) can be generalized as

$$j = 2\left(i - n_{sw}\left\lfloor \frac{i}{n_{sw}} \right\rfloor\right) - 1 + \left\lfloor \frac{i-1}{n_{sw}} \right\rfloor \tag{60}$$

$$k_{ij} = \begin{cases} \mathbb{I}(k) & \text{if } \kappa \le N_{bed} \\ \mathbb{P}(k) & \text{if } \kappa > N_{bed} \end{cases} \tag{61}$$

$$\kappa = \mathrm{mod}(i + 2j - 1, N_{bed}) + 1 \tag{62}$$

where $N_{bed} = 2n_{sw}$ in general.

3. Results and discussions

3.1. Standard four-bed simulation

3.1.1. Operation time scales

In this section, we investigate the performance of an AD system consisting of four beds. Using Eq. (47) and specific parameters in Table 2, we obtain $\tau_{sw} = 83.41 + 187.23\ \phi_{sw}$ [s], which indicates that the switching interval should be longer than (at least) 83.41 s. By experience we, learned that $\phi_{sw} = 0.15 - 0.20$ is a reasonable approximation and set $\tau_{sw} = 120$ s ($\phi_{sw} = 0.1976$) as an integer value for simplicity. The reaction time is set to be 1080 s to have the half cycle $\tau_{hc} = 1200$ s, which is 10 times the switching interval. To distinguish the elapsed time for each bed, we used the bed index ($i = 1 - 4$) as the subscript of physical variables.

Table 4
The index of bed k, denoted k_{ij}, if bed i advances $j\tau_{sw}$ in time. Bold numbers indicate physical pairs.

$i(=k_{i0})$	k_{i1}	k_{i2}	k_{i3}	k_{i4}	k_{i5}	k_{i6}	k_{i7}	k_{i8}
1	3	5	7	**2**	**4**	**6**	**8**	1
2	4	6	8	**1**	**3**	**5**	**7**	2
3	5	7	**2**	**4**	**6**	**8**	1	3
4	6	8	**1**	**3**	**5**	**7**	2	4
5	7	**2**	**4**	**6**	**8**	1	3	5
6	8	**1**	**3**	**5**	**7**	2	4	2
7	**2**	**4**	**6**	**8**	1	3	5	7
8	**1**	**3**	**5**	**7**	2	4	6	8

3.1.2. Initial and periodic variation of temperature profiles

Periodic variation of pressure and temperature profiles of the four-bed operation is shown in Fig. 6(a). Initially, beds 1 and 2 are in the precooling and preheating states, respectively. These beds have the first switching duration of $0 < t_1$ & $t_2 < \tau_{sw}$, being disconnected from the evaporator and the condenser. In this duration, the internal heat of bed 1 is exchanged with that of the cooling stream from the heat exchanger. This results in the rapid decrease in T_1, and similarly, T_2 promptly increases. Precooling of bed 1 and preheating of bed 2 occur in the n_c^{th} full cycle, i.e., $(n-1)\tau_{fc} < t_1 \& t_2 < (n-1)\tau_{fc} + \tau_{sw}$, where τ_{fc} is the full cycle (the duration of the opposite thermal states can be found by replacing t_1 and t_2 by $t_1 - \tau_{hc}$ and $t_1 - \tau_{hc}$, respectively). In the rest of the first half cycle after the switching duration, i.e., $\tau_{sw} < t_1 < \tau_{hc}$, beds 1 and 2 undergo adsorption and desorption, respectively, and will repeat the reactions in the n_c^{th} cycle during $(n-1)\tau_{fc} + \tau_{sw} < t_1$ and $t_2 < (n - \frac{1}{2})$. Subtraction of τ_{hc} by t_1 and t_2 in the above equation provides periodic durations for desorption of bed 1 and adsorption of bed 2. Having the precooling phase as an initial thermal state, bed 1 repeats the four sub-processes in a specific sequential order, of which durations are summarized in Table 5. During every half cycle, beds 1 and 2 swap their thermodynamic states. Similar analysis can be made for beds 3 and 4. In the first half cycle, bed 3 (and 4) is in the adsorption (and desorption) state during $0 < t_3$(and t_4) $< \tau_{hc} - \tau_{sw}$ and preheating (and precooling) during $\tau_{hc} - \tau_{sw} < t_3$(and t_4) $< \tau_{hc}$. Afterward, beds 3 and 4 exchange their roles by toggling the heating and cooling streams. During the first full cycle ($0 < t < \tau_{fc}$), the four beds undergo all the sub-processes of precooling, adsorption, preheating, and desorption with specifically preset initial states of duration τ_{sw} or τ_{srp}. To identify specific sub-process durations of all four beds, one can replace t_1 in Table 5 by $t_2 - \tau_{hc}$, $t_3 - (\tau_{hc} + \tau_{sw})$, and $t_4 - (\tau_{hc} - \tau_{sw})$ for beds 2, 3, and 4, respectively. This is because the current thermal state of bed 1 is equal to those of beds 2, 3, and 4 after time has passed by τ_{hc}, $\tau_{hc} + \tau_{sw}$, and $\tau_{hc} - \tau_{sw}$, respectively.

It is worth noting that temperature profiles of the evaporator and the condenser have a (temporal) periodicity of τ_{hc}, which is a half of the periodicity of the beds. This is because all the beds switch their current thermal state to their anti-thermal state every τ_{hc}. This can be visually

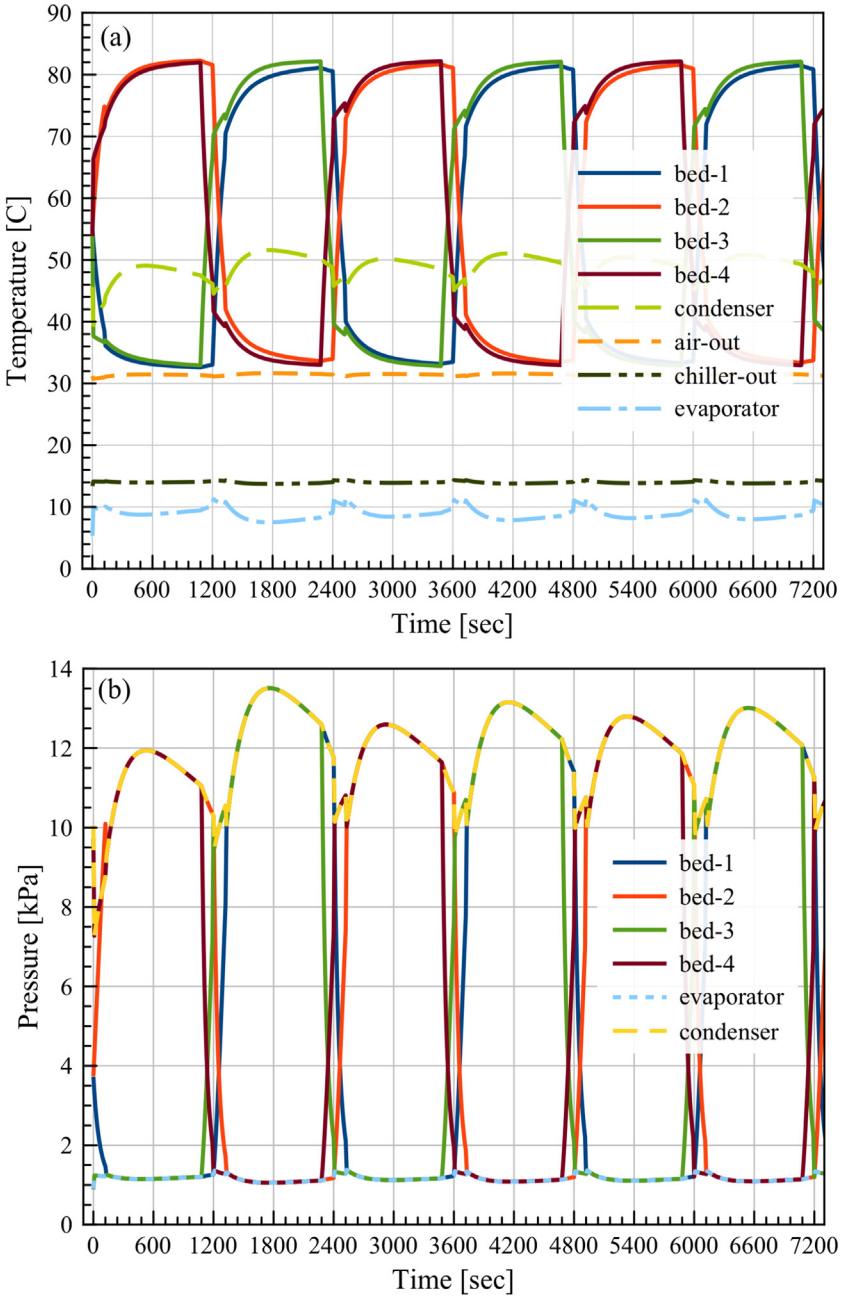

Fig. 6. (a) Temperature and (b) pressure profiles of the 4-bed operation. Parameters in Table 2 are used. The preprocessing and half-cycle times are set at 120 and 1200 s, respectively. The following initial conditions are used: $P_{bed,i} = 1.0$ kPa and $T_{bed,i} = 55$ °C for $i = 1 - 4$, $T_{evap} = 5$ °C, and $T_{cond} = 45$ °C. The temperature and pressure profiles become indifferent to the initial conditions after a few full cycles.

understood in Fig. 4. The evaporator and the condenser are connected to any two beds during $\max((n-1)\tau_{hc} - \tau_{sw}, 0) < t < (n-1)\tau_{hc} + \tau_{sw}$ and to four beds at other times, where n is an arbitrary positive integer. The number of beds connected to the evaporator and condenser changes from 4 to 2 at $t = \max((n-1)\tau_{hc} - \tau_{sw}, 0)$ and returns to 4 at $t = (n-1)\tau_{hc} + \tau_{sw}$. The condenser/evaporator temperatures in Fig. 6(a) show rapid variation near the above-mentioned specific instances. Table 6 lists durations and thermal states of the four beds in the first half cycle ($0 \le t \le \tau_{hc}$), which also gives the number of beds connected to the evaporator and the condenser. During Δt_1, only bed 3 is connected to the evaporator and only bed 4 to the condenser. Similarly, during Δt_3, only bed 1 (and 2) is connected to the evaporator (and the

Table 5
Sub-process durations of bed 1 with respect to time.

Bed no.	1
Precooling	$(n-1)\tau_{fc} < t_1 < (n-1)\tau_{fc} + \tau_{sw}$
Adsorption	$(n-1)\tau_{fc} + \tau_{sw} < t_1 < (n-\frac{1}{2})\tau_{fc}$
Preheating	$(n-\frac{1}{2})\tau_{fc} < t_1 < (n+\frac{1}{2})\tau_{fc} + \tau_{sw}$
Desoprtion	$(n+\frac{1}{2})\tau_{fc} + \tau_{sw} < t_1 < (n+1)\tau_{fc}$

Table 6
Sub-process of the four bed during the fist half-cycle.

Bed	$\Delta t_1 = \tau_{sw}$	$\Delta t_2 = \tau_{hc} - 2\tau_{sw}$	$\Delta t_3 = \tau_{sw}$
1	pcl	ads	ads
2	pht	des	des
3	ads	ads	pht
4	des	des	pcl

condenser), respectively. During Δt_1 and Δt_3, a quarter of the beds are connected to the evaporator, another quarter to the condenser, and the rest are isolated. During Δt_2, any bed is connected to either the evaporator or the condenser. In general, the quarter connection occurs at $\max((n-1)\tau_{hc}-\tau_{sw}) < t < (n-1)\tau_{hc}+\tau_{sw}$.

Immediately after $(n-1)\,\tau_{hc}+\tau_{sw}$, the condenser starts receiving hot vapor from half of the beds. The heat released inside the condenser suddenly increases the condenser temperature, reaching a maximum. Afterward, temperatures of desorption beds vary slowly and the vapor migration rate to the condenser gradually decreases as pre-adsorbed water in the desorption beds is continuously depleted. The condenser temperature T_{cond} rapidly reaches its maximum and then gradually decreases until time reaches $n\tau_{hc}-\tau_{sw}$. Temporal variation of the evaporator shows the opposite trend to that of the condenser in Fig. 6. The evaporator temperature rapidly decreases, reaches a minimum, and gradually increases while the condenser temperature promptly increases, reaches a maximum, and slowly decreases.

3.1.3. Initial and periodic variation of pressure profiles

Fig. 6(b) shows pressure profiles of the four beds, evaporator, and condenser. When the time is around a multiple of the half cycle (τ_{hc} = 1,200 s), all four beds show rapid variations in their pressure profiles. This is because the beds either enter or leave switching states before or after every half cycle. (Similar trends are found in the bed temperature profiles shown in Fig. 6(a).) In adsorption and desorption states, the bed pressure is set equal to those of the evaporator and condenser, respectively. These are shown as the lower and upper bounds of Fig. 6(b), respectively. This pressure-bounding is already explained in the $P-T-\phi$ diagram of Fig. 3. The bed temperature is influenced primarily by the heat transfer rates of heat-exchanging water streams and secondarily by the heat consumption rates for adsorption or desorption of water (adsorbate). In other words, the bed pressure is mainly controlled by the gaseous vapor concentration and secondarily by the bed temperature, which changes the kinetic energy of gas molecules in the beds. The response of the bed pressure to the incoming heat-exchanging streams is via that of the bed temperature. This results in slower periodic convergence of the bed pressure profiles shown in Fig. 6(b), compared to those of bed temperatures, shown in Fig. 6(a), promptly reaching a stable periodic state after one or two full cycles. Due to the indirect influence of the heat-exchanging fluid temperatures, it takes a (little) longer time for the bed pressure to be periodically stabilized.

3.2. Initial time lag

3.2.1. Four-bed case

In every $\max((n-1)\tau_{hc}-\tau_{sw}) < t < (n-1)\tau_{hc}+\tau_{sw}$ for a positive integer n, each bed undergoes either precooling or preheating. Therefore, one can set the half cycle as an integer of $2\tau_{sw}$, i.e.,

$$\tau_{hc} = m(2\tau_{sw}) \tag{63}$$

and equivalently $n_{sw} = 2m$ in Eq. (51), where m is a positive integer. For the case studied in Fig. 6, we already used $m = 5$. Then, the duration in which all the four beds are in reaction states is $(m-1)(2\tau_{sw})$ within a half cycle. Fig. 4 indicates that the states of beds 3 and 4 are τ_{hc} faster than those of beds 1 and 2, respectively. For example, if bed 3 currently starts preheating now, bed 1 will be in preheating in τ_{sw} later. Here, one can write

$$t_{i+2} = t_i + \tau_{sw} \tag{64}$$

indicating that bed $i(=1,2)$ will be in the same state of bed $i+2$ after τ_{sw}. Eq. (64) is an equivalent representation of Eq. (50). Here, we define the initial time lag (ITL) of beds 3 and 4 as

$$\mathrm{ITL} = t_{i+2} - (t_i - \tau_{sw}) = l\tau_{sw} \tag{65}$$

where l, defined as dimensionless ITL, is from 0 to $2m-1$. If $l = 0$, the time sequences of the four beds is found in Fig. 4. If $l = 1$, then the time sequences of beds 3 and 4 move to the right as much as τ_{sw} and therefore beds 1 and 3 will have exactly the same thermal state at any time t, similarly for beds 2 and 4. The maximum meaningful value of l is $2m-1$, because $l = 2m$ is equivalent to $k = 0$ due to the periodic characteristic of the AD process. Fig. 7(a) shows the performance of the 4-bed AD system in terms of COP, SCC, and SDWP with respect to the dimensionless ITL, l, from 0 to $4m$ while $m = 5$. A full cycle is for l from 0 to $4m-1$ and therefore the first half cycle from $k = 0$ to 9 and the second from $l = 10$ to 19. To clarify the boundary between two half cycles, data points are disconnected in Fig. 7 between $l = 9$ and 10. In Fig. 7(a), values at $l = 0$, 10, and 20 are identical, which indicates intrinsic periodicity of the AD process. Interestingly, we observed that COP and SCC are symmetric about $l = 9$ over the full cycle. In other words, values of COP and SCC at l and $l'(=18-l)$ are equal to each other: for example, those of $(l,l') = (8,10),(4,14)$, and $(1,17)$ are all equal. Over half cycles, COP and SCC are symmetric about $l = 4$ and 14, whose sum is also 18. Unlike COP and SCC, SDWP does not show any symmetric behavior, but translational invariance. Two SDWP values at l and $l'(=l+2m)$ are identical to each other for l from 0 to 10. Interestingly, the peak values of SDWP are found at $l = 7$ and $l'(=l+2m) = 17$ after monotonous increases for $1 < l < 7$ and $11 < l < 17$. Within a half cycle, the peak position of SDWP is off-set by 1 with that of COP and matched to the second peak positions of SCC. The SWDP value increases 11% from $l = 0$ to $l = 7$ where both COP and SCC recover to their values of $l = 0$. Fig. 7(a) gives a promising potential of using ITL of the second bed-pair in the four-bed AD system to control the relative performance of SWDP over COP and SCC.

3.2.2. Six-bed case

Fig. 7(b) shows the performance of 6-bed AD operations. All basic parameters used are same as those used for 4-bed operation, listed in Table 2. Two more beds are added as beds 5 and 6 to the previous 4-bed configuration. In this case, the AD system consists of three independent bed-pairs. At any time, bed i and $i+1$ for $i = 1,3,5$ form a pair of thermally opposite states. Without ITL, beds 1 and 2 are in precooling and preheating states, respectively; beds 3 and 4 are in adsorption and desorption states, respectively; and importantly, beds 5 and 6 are in the same states of beds 1 and 2, respectively. The ITL of the third pair (beds 5 and 6) is twice the ITL of the second pair (beds 3 and 4). For example, if beds 3 and 4 have ITL of $2\tau_{sw}$ (=240 s), then beds 5 and 6 have ITL of $4\tau_{sw}$ (=480 s). Fig. 7(b) shows performances of a 6-bed AD system with respect to the dimensionless ITL, l, running from 0 to 9. Similar to the 4-bed case, COP and SCC of the 8-bed system show symmetric trends about $l = 5$. SDWP monotonously increases from $l = 0$ to 9 with locally fluctuating behavior. Increases in SDWP over this range is >20%. Interestingly, all of the three performance coefficients have maximum values at $l = 9$. Having the third pair (of beds 5 and 6), whose initial thermal states are identical to those of beds 1 and 2, respectively, the 6-bed AD system shows a higher COP at $l = 1$ than that at $l = 0$. In both cases, any two beds are in a same thermal state, i.e., beds 1 and 5 at $l = 0$ and beds 1 and 3 at $k = 1$. The thermal sequence of bed 5 of $l = 1$ is off-set by $2\tau_{sw}$, but that of bed 3 at $l = 0$ is offset by τ_{sw}. In the time sequence span, the switching intervals are less localized in $l = 1$ case than $l = 0$ case, giving a higher COP value as shown in Fig. 7(a).

3.2.3. Eight-bed cases with two different bed groups

Although Fig. 7(b) shows interesting results using 6 beds, thermal phases of 8 beds can have better periodic and symmetric characteristics in the performance evaluation. Results are shown in Fig. 8(a) and (b) for $N_{group} = 2$ and 4, respectively. Here, N_{group} indicates the number of beds in a group having the same ITL. The standard configuration of eight beds consists of the four beds shown in Fig. 4 ($l = 0$) plus a cloned set of the four beds. The second set of beds will be 5 to 8.

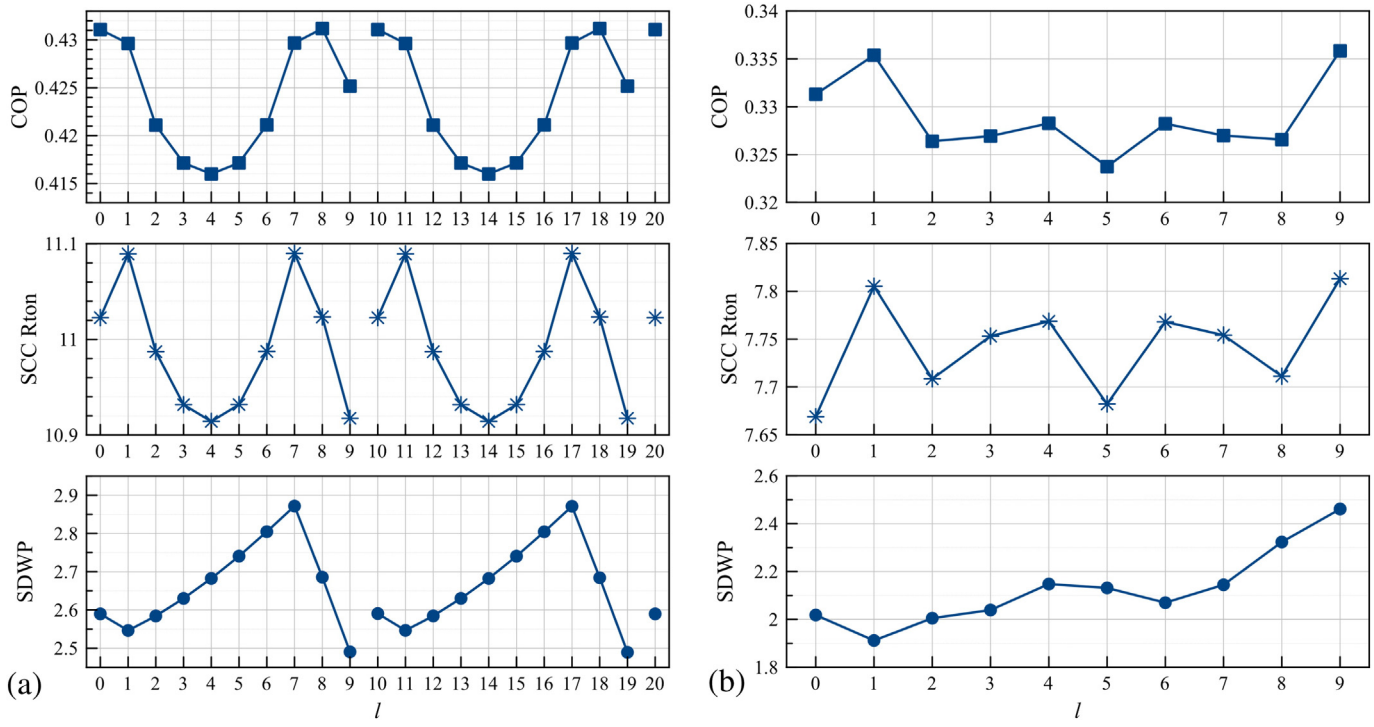

Fig. 7. Effects of the dimensionless ITL (l) on COP, SCC and SDWP of (a) 4-bed and (b) 6-bed AD operations with $N_{group} = 2$. A unit l indicates the switching interval τ_{sw}(=120 s).

If $l = 1$ for $N_{group} = 2$, then the thermal states of beds 3 and 4 move $\tau_{sw}$to the right, those of beds 5 and 6 move $2\tau_{sw}$to the right, and finally those of beds 7 and 8 are $3\tau_{sw}$to the right. In this very special case, all eight beds will be simultaneously in switching or sorption phases. COP, SCC, and SDWP trends of the eight beds with respect to the dimensionless ITL l are similar to those of six beds. The inefficient timing of $l = 1$ of $N_{group} = 2$ gives a drastic decrease in SDWP, but COP and SCC vary smoothly. In this $N_{group} = 2$ case, i.e., where two beds form a group, this 8-bed AD system often provides physically meaningless numerical results if $l > 6$. Fig. 8(b) shows the performance of 8 beds with $N_{group} = 4$, indicating each of 4 beds forms a group of a same ITL. For $l = 0$, two cases of $N_{group} = 2$ and 4 give identical results in Fig. 8(a) and (b). If $l = 2$, thermal states of the second bed group (beds 5–8) move $2\tau_{sw}$ to the right in the time sequence diagram. Unlike $N_{group} = 2$ case, smoothly varying COP, SCC, and SDWP are observed with respect to l. Interestingly, COP and SCC show symmetric behavior about $l = 10$ for

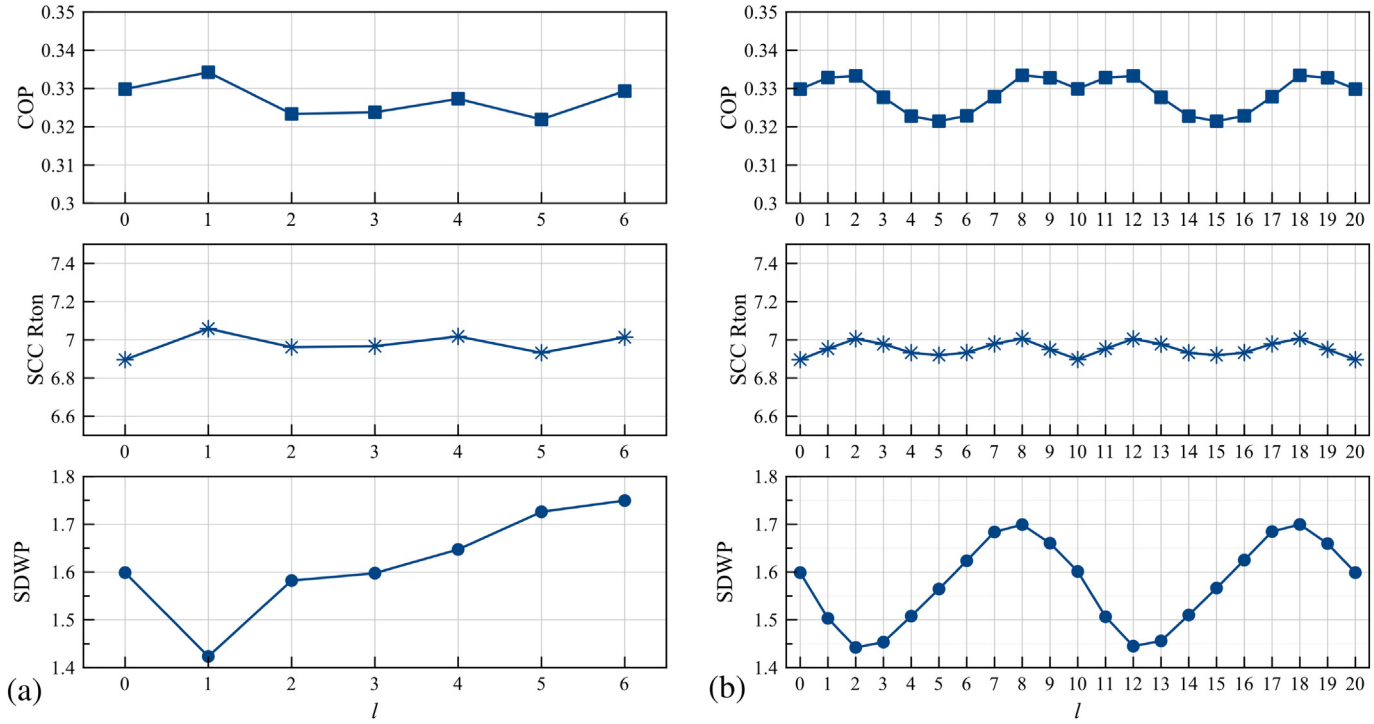

Fig. 8. Effects of the dimensionless ITL (l) on COP, SCC and SDWP of 8-bed AD operations with (a) $N_{group} = 2$, and (b) $N_{group} = 4$. A unit l indicates the switching interval τ_{sw}(=120 s).

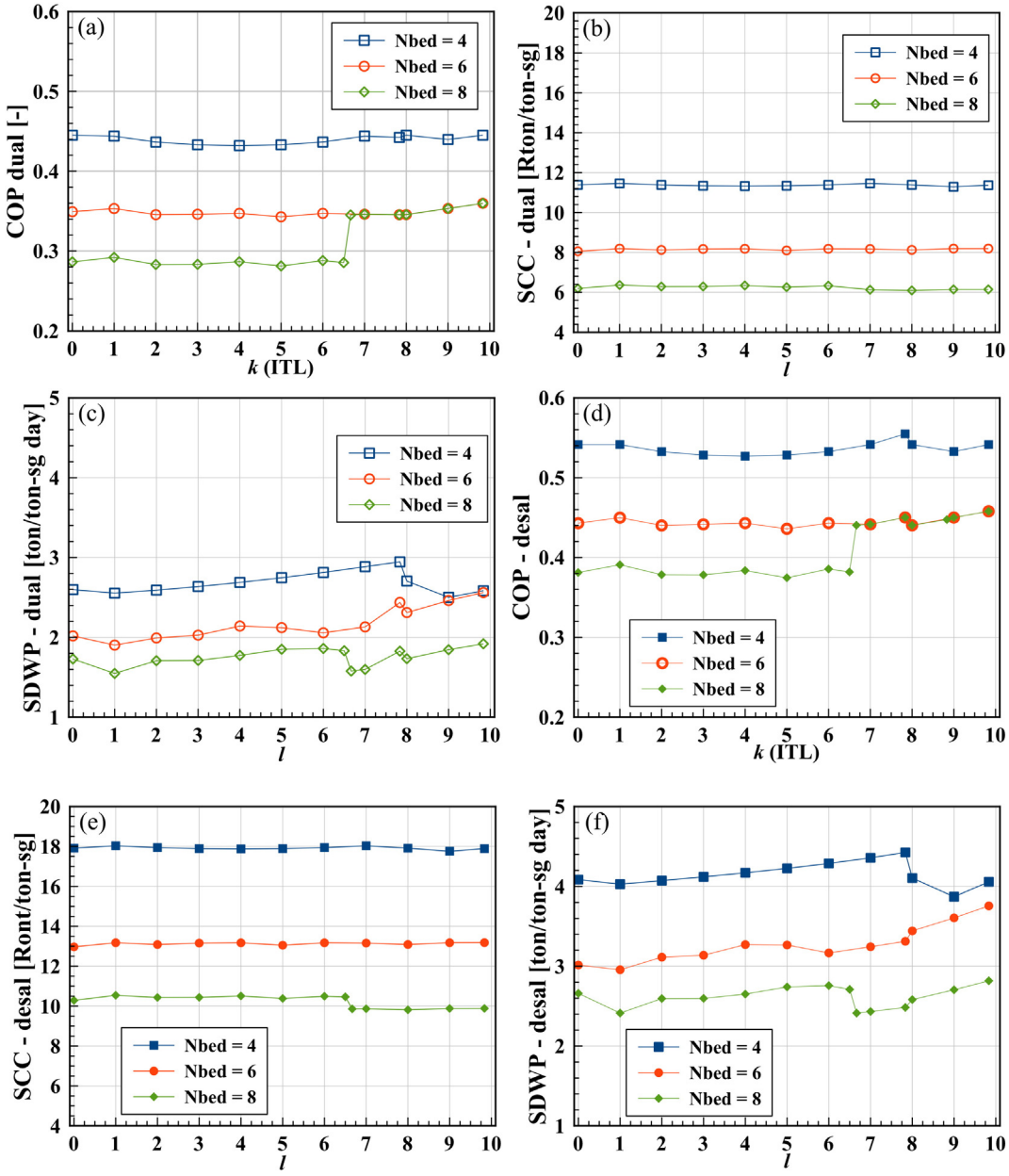

Fig. 9. (a) coefficient of performances, (b) specific cooling capacity, and (c) specific daily water production rate in the dual mode; and (d) coefficient of performances, (e) specific cooling capacity, and (f) specific daily water production rate in the desalination mode, with respect to the dimensionless ITL (l).

full cycles and $k = 5$ and 15 for half cycles. Only SDWP shows translational invariance in time with periodicity of $l = 10$. Figs. 7(a) and 8(b) have two bed groups with $N_{group} = 4$, and Figs. 7(b) and 8(a) have four bed groups with $N_{group} = 2$. Comparing Figs. 7 and 8, we observe that two bed groups provide more stable and controllable performance by changing the dimensionless ITL, l.

3.3. Dual and desalination modes of 8-bed AD system

Fig. 9 shows performance of systems consisting of 4, 6, and 8 soprtion beds in terms of COP, SDWP, and SCC. Two modes are studied in this case: dual and desalination modes. The former uses the same chiller temperature of $T_{ch,in} = 15$ °C and the latter uses $T_{ch,in} = 30$ °C.

Fig. 9(a) shows variations of COP of multiple beds in the dual mode with respect to the dimensionless ITL. Overall, COP decreases with respect to the number of beds, N_{bed}. This is because the common heat resources of the evaporator and the condenser (inputs and outputs) are evenly shared by all the beds. COP curves of three cases of N_{bed}(=4,6, and 8) show almost plateau trends. Interestingly, 8-bed COP suddenly jumps at l around 6.5 and afterward becomes very close to that of the 6-bed. This indicates that if the ITL is properly selected, then the performance of a multi-bed AD system can be noticeably enhanced without using additional energy. Fig. 9(b) shows flat profiles of SCCs, which do not show any noticeable changes near the special $l \simeq 6.5$ and 8. The COP jump of the 8-bed AD system is accompanied by a slight decrease in its SDWP as shown in Fig. 9(c). Unlike COP and SCC, SDWP of the 4-bed AD system gradually reaches a peak at $l = 8$ and decreases to its value of $l = 0$. The same quick decreases are found for $N_{bed} = 6$ and 8 cases as well at $l = 8$. Interestingly, after $l = 8$, SDWPs of 6- and 8-bed AD systems continuously increase. In this dual mode described above, $T_{ch,in} = 15$ °C is used to have $T_{ch,out}$ low enough for extra cooling. As the evaporation rate is proportional

to $T_{ch,in}$, a higher $T_{ch,in}$ will significantly enhance SDWP if water production is of more importance. In this case, one can have $T_{ch,in} = 30$ °C, which is called the desalination mode in this study, keeping all other parameters identical to those of the dual mode. COP, SCC, and SDWP of the desalination mode are shown in Fig. 9(d)–(f), respectively.

In comparison to COP of the dual mode, Fig. 9(d) shows higher COP in the desalination mode. The COP jump of 8-bed AD system is also shown in this desalination mode, which is proven to be independent of $T_{ch,in}$. In general, variations of COP with respect to l in the desalination mode are slightly more noticeable than in the dual mode. Similar to SCCs of the dual mode shown in Fig. 9(b), those of the desalination mode show plateau trends in Fig. 9(e). One small exception is the SDWP of 8-bed case near $l \simeq 6.5$ where a small change is presented. In each case of N_{bed}, the desalination mode shows higher SCC than that of the dual mode. In Fig. 9(f), SDWP of 4-bed case in the desalination mode shows higher magnitude than that in the dual mode, and the same trend is found where it gradually increases, reaches a peak value, and then decreases to its value of no ITL. SDWPs of 6- and 8-bed case in the desalination mode show very similar trends to those in the dual mode, having higher magnitudes. Specifically at $l = 8$, SDWP of 6- and 8-bed cases shortly increase in the desalination mode, but in general decrease in the dual mode. Although the magnitudes of these SDWP changes are small in the two modes, the trends are opposite.

4. Conclusion

In this work, we re-investigated the standard adsorption desalination (AD) process and developed a formalism of thermal energy transfer between individual units. We generalized heat transfer rate expressions of the evaporator, the condenser, and the sorption beds at an arbitrary thermal state using mathematical on/off functions. The critical pressure is mathematically defined as Eq. (5). Conventionally, the optimal intervals of switching and reactions are determined by experimental trial and error or educated guess by researchers' experiences. We developed an analytic equation (Eq. (47)) to estimate the minimum time-interval for the periodic switching process. Our estimation of the switching interval is in reasonably good agreement with values reported in literature. To the best of our knowledge, we are the first to introduce the concept of the initial time lag of the thermodynamic phases of paired beds and show its practical potential to control the relative performance of cooling and desalination.

Performance of a 4-bed operation was investigated in terms of COP, SCC, and SDWP with respect to the dimensionless ITL (k_{ITL}), making a group with 2 beds. This simplest ITL scheme shows quasi-symmetric behaviors in COP and SCC and a left-skewed trend in SDWP. The 6-bed ITL of the same setup shows almost identical trends to those of 4-bed ITL operations. These results clearly show the practical potential of ITL to increase SDWP or specifically control relative magnitudes of COP, SCC and SDWP. The ITL application to 8-bed shows that grouping 4 beds (instead of 2 beds) provides more stable and predictable variations of the performance coefficients with respect to the dimensionless ITL as compared to those of grouping 2 beds.

Based on the standard 4-bed operation analysis, we investigated effects of the initial time lags on 4,- 6-, and 8-bed performance in terms of COP, SCC and SDWP with $N_{group} = 2$. Interestingly, the COP jump is observed at a specific value of k_{ITL}, where SDWP quickly decreases with a small magnitude. This signifies that the optimal value of k_{ITL} gives higher COP than expected with no ITL. Although SDWP decreases with respect to the number of beds, N_{bed}, the total amount of water produced per day, as a multiplication of SDWP and N_{bed}, noticeably increases. The desalination mode of high $T_{ch,in}$ shows a special application of AD only for clean water production without any cooling capability. Increasing $T_{ch,in}$ from 15 °C to 30 °C increases all the performance coefficients by approximately 50%. This specifically indicates that the desalination mode can produce water >1.5 times in a given duration than the dual mode. The trade-off is zero cooling capacity. As discussed above, the potential of using ITL is very promising in practical operations, because changing ITL can give us great flexibility in controlling relative performance of heat and mass transfer rates.

Nomenclature

Roman symbols

$\dot{m}$	mass flow rate [kg/s]
$\mathcal{R}$	univeral gas constant of water [kJ/kg]
A	area [m^2]
$c_{p,a}$	specific heat capacity of air, 1.005 [kJ/kg·K]
$c_{p,s}$	specific heat capacity of solid [kJ/kg·K]
$c_{p,w}$	specific heat capacity of water, 4.184 [kJ/kg·K]
c_p	specific heat capacity [kJ/kg·K]
H	heat rate [kJ/s]
h	enthalpy [kJ/kg]
M	mass [kg]
P	pressure [kPa]
p_{sat}	saturation pressure of water [kPa]
Q_{st}	specific heat of adsorption [kJ/kg]
S	entropy [kJ/kg K]
T	temperature [K]
t	time [*sec*]
U	overall heat transfer coefficient [$kW/m^2 \cdot K$]

Greek symbols

ϕ	uptake ratio [kg/kg]

Subscripts/superscripts

ads	adsorption
approx	approximation
a	air
bed	reaction bed
ch	chilled water
cond	condenser
crit	critical
cw	cold water
cyc	cycle
des	desorption
eff	effective
evap	evaporator
ff	feed flow
fg	fluid to gas
f	feed
g	gas
hw	hot water
hx	heat exchanger
in	input
out	output
pcl	precooling
pht	preheating
rxn	reaction, i.e., adsorption and/or desorption
sg	silica gel
srp	adsorption or desorption
sw	switching
w	water

Acknowledgement

This work was financially supported by the R&D project of "Infrastructure Establishment of Thermal Energy Conversion and Desalination using Seawater Thermal Energy" (PES2310) from Korea Research Institute of Ships and Ocean Engineering (KRISO) and by the National R&D project of "Development of new application technology for deep seawater industry" (PMS3380) from the Ministry of Oceans and Fisheries of the Republic of Korea.

Appendix A

A.1. Entropy change

Fig. 3 shows phase paths of the four AD subprocesses, each of which is assumed to be in a quasi-equilibrium state. Since entropy is a thermodynamically additive quantity, total entropy of AD process (S) can be written as a superposition of entropies of adsorbed (S_a) and solid (S_s) phases:

$$S = S_a + S_s \tag{66}$$

In each subprocess, S must change with respect to P, T, and ϕ:

$$\mathrm{d}S = \left(\frac{\partial S_a}{\partial T} + \frac{\partial S_s}{\partial T}\right)\mathrm{d}T + \frac{\partial S_a}{\partial P}\mathrm{d}P + \frac{\partial S_a}{\partial \phi}\mathrm{d}\phi \tag{67}$$

where S_s is assumed to be indifferent to P and ϕ. Chakraborty et al. [30] derived the entropy change as

$$\mathrm{d}S = \left(\frac{c_{p,s} + c_{p,a}}{T}\right)\mathrm{d}T - \left(\frac{\partial v_a}{\partial T}\right)_{P,\phi}\mathrm{d}P + \left[S_g - \frac{Q_{\mathrm{st}}}{T}\right]\mathrm{d}\phi \tag{68}$$

where $c_{p,s}$ and $c_{p,a}$ are specific heat capacities of the solid and adsorbed phases, respectively, S_g is entropy of the gas phase, Q_{st} is expressed in Refs. [31] and [32] as

$$Q_{\mathrm{st}} = T(v_g - v_a)\frac{\mathrm{d}P}{\mathrm{d}T} \tag{69}$$

and v_g and v_a are the specific volume of gas and adsorbed phases, respectively.

Precooling and preheating states are isosteric ($\mathrm{d}\phi = 0$) in a quasi-equilibrium state so that Eq. (68) can be rewritten as

$$\frac{\mathrm{d}S_{\mathrm{pcl/pht}}}{\mathrm{d}T} = \left(\frac{c_{p,s} + c_{p,a}}{T}\right) - \left(\frac{\partial v_a}{\partial T}\right)_{P,\phi}\frac{\mathrm{d}P}{\mathrm{d}T} \tag{70}$$

where $\mathrm{d}P/\mathrm{d}T$ indicates a gas-phase pressure change with respect to bed temperature, following the Clausius-Clapeyron equation. The first term on the right side of Eq. (70) is dominant because a (hot or cold) heat-exchanging stream is the sole major heat source or sink for the bed. The second term is simply feedback due to subsequent pressure change. As the temperature continuously decreases/increases in the precooling/preheating state, entropy decreases/increases accordingly. Then, one can write

$$\frac{\mathrm{d}S_{\mathrm{pcl}}}{\mathrm{d}T} = -\frac{\mathrm{d}S_{\mathrm{pht}}}{\mathrm{d}T} < 0 \tag{71}$$

or

$$\mathrm{d}(S_{\mathrm{pcl}} + S_{\mathrm{pht}}) = 0 \tag{72}$$

indicating that the quasi-equilibrium assumption makes the precooling/preheating states thermodynamic path-independent.

Adsorption and desorption processes are isobaric ($\mathrm{d}P = 0$) in a quasi-equilibrium state. Therefore, similar to the entropy changes of Eq. (70) in the preprocessing states, one can write, for reaction states

$$\frac{\mathrm{d}S_{\mathrm{ads/des}}}{\mathrm{d}T} = \left(\frac{c_{p,s} + c_{p,a}}{T}\right) + \left[S_g - \frac{Q_{\mathrm{st}}}{T}\right]\frac{\mathrm{d}\phi}{\mathrm{d}T} \tag{73}$$

Because $\mathrm{d}\phi/\mathrm{d}T < 0$, entropy reaches its minima and maxima at the end of adsorption and desorption periods, respectively. The second term on the right side of Eq. (73) indicates a subsequent change in the amount of adsorbed adsorbate due to the bed temperature change. Similar to the preprocessing states, $S_{\mathrm{ads/des}}$ is assumed as path-independent so that

$$\frac{\mathrm{d}S_{\mathrm{ads}}}{\mathrm{d}T} = -\frac{\mathrm{d}S_{\mathrm{des}}}{\mathrm{d}T} < 0 \tag{74}$$

or

$$\mathrm{d}(S_{\mathrm{ads}} + S_{\mathrm{des}}) = 0 \tag{75}$$

Finally, Eqs. (72) and (75) indicate that the total entropy is conserved:

$$\mathrm{d}S = \mathrm{d}(S_{\mathrm{pcl}} + S_{\mathrm{pht}} + S_{\mathrm{ads}} + S_{\mathrm{des}}) = 0 \tag{76}$$

Again, this is because in our theoretical development each subprocess is assumed to be in a thermodynamically quasi-static equilibrium. In actual AD operations, the total entropy change should be positively finite

$$\mathrm{d}S \geq 0 \tag{77}$$

and will eventually increase because

1. the AD system is intrinsically transient without reaching any steady state,
2. the bed temperature rapidly changes especially at the beginning of preprocessing periods, and
3. the bed wall is, generally speaking, not a perfect thermal insulator, dissipating thermal energies.

See Section 2.3 for detailed entropy analysis for each subprocess.

References

[1] Department of Economic and Social Affairs, Population Division, United Nations, World Population Prospects: The 2015 Revision, 2015 1–66.
[2] Bureau of Inernational Information Programs, United States Deparment of State, Global Water Issues, Tech. Rep. 2011.
[3] 2030 Water Resource Group, Charting Our Water Future, Tech. Rep., 2009.
[4] J.E. Miller, Review of Water Resources and Desalination Technologies, Sandia National Laboratories, SAND-2003-0800, Tech. Rep., 2003.
[5] K. Thu, A. Chakraborty, B.B. Saha, W.G. Chun, K.C. Ng, Life-cycle cost analysis of adsorption cycles for desalination, Desalin. Water Treat. 20 (1–3) (2012) 1–10.
[6] K. Thu, G. Amy, K.C. Ng, Y. Kim, A. Chakraborty, Adsorption desalination: an emerging low-cost thermal desalination method, Desalination 308 (2013) 161–179.
[7] M. Sivak, Will AC put a chill on the global energy supply? Am. Sci. 101 (5) (2013) 330–333.
[8] L.W. Davis, P.J. Gertler, Contribution of air conditioning adoption to future energy use under global warming, Proc. Natl. Acad. Sci. 112 (19) (2015) 5962–5967.
[9] K. Birgersson, P. Balaya, S. Chou, J. Yan, Energy solutions for a sustainable world, Appl. Energy 90 (1) (2012) 1–2.
[10] N. Ghaffour, S. Lattemann, T. Missimer, K.C. Ng, S. Sinha, G. Amy, Renewable energy-driven innovative energy-efficient desalination technologies, Appl. Energy 136 (2014) 1155–1165.
[11] K.C. Ng, K. Thu, A. Chakraborty, B.B. Saha, W.G. Chun, Solar-assisted dual-effect adsorption cycle for the production of cooling effect and potable water, Int. J. Low Carbon Technol. 4 (2) (2009) 61–67.
[12] S.M. Sami, C. Tribes, An improved model for predicting the dynamic behaviour of adsorption systems, Appl. Therm. Eng. 16 (2) (1996) 149–161.
[13] H.T. Chua, K.C. Ng, A. Malek, T. Kashiwagi, A. Akisawa, B.B. Saha, Modeling the performance of two-bed, silica gel-water adsorption chillers, Int. J. Refrig. 22 (3) (1999) 194–204.
[14] H.T. Chua, K.C. Ng, W. Wang, C. Yap, X.L. Wang, Transient modeling of a two-bed silica gel–water adsorption chiller, Int. J. Heat Mass Transf. 47 (4) (2004) 659–669.
[15] K. Thu, A. Chakraborty, Y.-D. Kim, A. Myat, B.B. Saha, K.C. Ng, Numerical simulation and performance investigation of an advanced adsorption desalination cycle, Desalination 308 (2013) 209–218.
[16] T. Miyazaki, T. Miyazaki, A. Akisawa, B.B. Saha, B.B. Saha, A. Akisawa, I.I. El-Sharkawy, A. Chakraborty, I.I. El-Sharkawy, A. Chakraborty, A new cycle time allocation for enhancing the performance of two-bed adsorption chillers, Int. J. Refrig. 32 (5) (2009) 846–853.
[17] B.B. Saha, S. Koyama, J.B. Lee, K. Kuwahara, K.C.A. Alam, Y. Hamamoto, A. Akisawa, T. Kashiwagi, Performance evaluation of a low-temperature waste heat driven multi-bed adsorption chiller, Int. J. Multiphase Flow 29 (8) (2003) 1249–1263.
[18] K.C.A. Alam, Y.T. Kang, B.B. Saha, A. Akisawa, T. Kashiwagi, A novel approach to determine optimum switching frequency of a conventional adsorption chiller, Energy 28 (10) (2003) 1021–1037.

[19] K. Thu, Y.-D. Kim, G. Amy, W.G. Chun, K.C. Ng, A hybrid multi-effect distillation and adsorption cycle, Appl. Energy 104 (2013) 810–821.
[20] M.W. Shahzad, K. Thu, Y.-d. Kim, K.C. Ng, An experimental investigation on MEDAD hybrid desalination cycle, Appl. Energy 148 (2015) 273–281.
[21] J.W. Wu, E.J. Hu, M.J. Biggs, Thermodynamic cycles of adsorption desalination system, Appl. Energy 90 (1) (2012) 316–322.
[22] J.W. Wu, M.J. Biggs, P. Pendleton, A. Badalyan, E.J. Hu, Experimental implementation and validation of thermodynamic cycles of adsorption-based desalination, Appl. Energy 98 (2012) 190–197.
[23] K. Thu, Y.-D. Kim, M.W. Shahzad, J. Saththasivam, K.C. Ng, Performance investigation of an advanced multi-effect adsorption desalination (MEAD) cycle, Appl. Energy 159 (2015) 469–477.
[24] Y.-D. Kim, K. Thu, K.C. Ng, Adsorption characteristics of water vapor on ferroaluminophosphate for desalination cycle, Desalination 344 (2014) 350–356.
[25] Y.-D. Kim, K. Thu, M.E. Masry, K.C. Ng, Water quality assessment of solar-assisted adsorption desalination cycle, Desalination 344 (2014) 144–151.
[26] J. Toth, State equations of the solid-gas interface layers, Acta Chim. Acad. Sci. Hung. 69 (1971) 311–328.
[27] H.T. Chua, K.C. Ng, A. Chakraborty, N.M. Oo, M.A. Othman, Adsorption characteristics of silica gel + water systems, J. Chem. Eng. Data 47 (5) (2002) 1177–1181.
[28] S. Mitra, K. Srinivasan, P. Kumar, S.S. Murthy, P. Dutta, Solar driven adsorption desalination system, Energy Procedia 49 (2014) 2261–2269.
[29] A.S. Kim, A two-interface transport model with pore-size distribution for predicting the performance of direct contact membrane distillation (DCMD), J. Membr. Sci. 428 (2013) 410–424.
[30] A. Chakraborty, B.B. Saha, S. Koyama, K.C. Ng, K. Srinivasan, Adsorption thermodynamics of silica gel-water systems, J. Chem. Eng. Data 54 (2) (2009) 448–452.
[31] H. Pan, J.A. Ritter, P.B. Balbuena, Examination of the approximations used in determining the isosteric heat of adsorption from the Clausius-Clapeyron equation, Langmuir 14 (21) (1998) 6323–6327.
[32] A. Chakraborty, B.B. Saha, S. Koyama, K.C. Ng, On the thermodynamic modeling of the isosteric heat of adsorption and comparison with experiments, Appl. Phys. Lett. 89 (2006) 171901.